

PNNL-31985

Critical Interference Mechanisms for Marine Renewable Energy-powered Ocean Observing Platforms

9/30/21

Emma Cotter

James McVey

DISCLAIMER

This report was prepared as an account of work sponsored by an agency of the United States Government. Neither the United States Government nor any agency thereof, nor Battelle Memorial Institute, nor any of their employees, makes **any warranty, express or implied, or assumes any legal liability or responsibility for the accuracy, completeness, or usefulness of any information, apparatus, product, or process disclosed, or represents that its use would not infringe privately owned rights.** Reference herein to any specific commercial product, process, or service by trade name, trademark, manufacturer, or otherwise does not necessarily constitute or imply its endorsement, recommendation, or favoring by the United States Government or any agency thereof, or Battelle Memorial Institute. The views and opinions of authors expressed herein do not necessarily state or reflect those of the United States Government or any agency thereof.

PACIFIC NORTHWEST NATIONAL LABORATORY
operated by
BATTELLE
for the
UNITED STATES DEPARTMENT OF ENERGY
under Contract DE-AC05-76RL01830

Printed in the United States of America

Available to DOE and DOE contractors from the
Office of Scientific and Technical Information,
P.O. Box 62, Oak Ridge, TN 37831-0062;
ph: (865) 576-8401
fax: (865) 576-5728
email: reports@adonis.osti.gov

Available to the public from the National Technical Information Service
5301 Shawnee Rd., Alexandria, VA 22312
ph: (800) 553-NTIS (6847)
email: orders@ntis.gov <<https://www.ntis.gov/about>>
Online ordering: <http://www.ntis.gov>

Critical Interference Mechanisms for Marine Renewable Energy-powered Ocean Observing Platforms

9/30/21

Emma Cotter

James McVey

Prepared for
the U.S. Department of Energy
Under Contract DE-AC05-76RL01830

Pacific Northwest National Laboratory
Richland, Washington 99352

Contents

1.0	Executive Summary	1
2.0	Introduction & Background	2
2.1	Overview of MRE Interference Mechanisms	2
2.1.1	Electrical	2
2.1.2	Acoustic	2
2.1.3	Motion	3
2.2	Use Cases	3
3.0	Use Case 1: Tidal-powered Passive Acoustic Monitoring	4
3.1	Acoustic Emissions from Tidal Turbines	5
3.2	Marine Mammal Vocalizations	7
3.3	Passive acoustic monitoring ranges	7
3.4	Detection range in the presence of a turbine	8
3.5	Turbulence-induced pseudosound	9
3.6	Discussion and Recommendations	12
4.0	Use Case 2: Wave-powered measurements of wavefields	14
4.1	Introduction	14
4.2	Field Measurements of Ocean Waves	14
4.3	Interference from Wave Energy Converters	18
4.3.1	WEC-influenced Wavefields	18
4.3.2	Point Absorber Wave Measurements	20
4.4	Discussion and Recommendations	22

Figures

1	Maximum turbine SPL at 1 m in the 1 kHz decidecade band as a function of maximum orca detection range and separation distance between the turbine and the hydrophone. Note that where ambient noise levels exceed turbine noise, ambient noise will limit detection rather than turbine noise.	10
2	a) Turbulent kinetic energy dissipation ratio (ϵ) in the Kvichak river during operation of the RivGen turbine (from Thomson and Guerra 2018, b) mean horizontal velocity during operation of the RivGen turbine (from Thomson and Guerra 2018, c) estimated pressure spectra from flow noise at 1 kHz using Equation 5, and d) difference between the estimated pressure spectra and a reference point, indicated by the black dot.	11
3	Estimated difference between flow noise in the Kvichak river at 1 kHz before installation of the RivGen turbine and while the turbine was operational, using data from Thomson and Guerra 2018	12
4	Data comparison between a commercial Waverider buoy's and a custom-built drifter buoy's vertical spectra, showing the characteristic f^{-4} slope (Pearman et al. 2014)	16
5	f^{-4} dependence and "check factor" quality control check. Bad data is where the check factor is greater than 1. (Thomson et al. 2015)	17
6	Commercial Datawell wave buoys (Herbers et al. 2012)	17
7	Buoy mooring diagrams (a.) NDBC DART buoy mooring (Teng 2002) (b.) Datawell buoy mooring (Thomson et al. 2013).	18
8	Nortek AWAC mounted in a bottom lander & a Datawell Waverider buoy (Pedersen and Lohrmann 2004)	19
9	(a.) An example wave energy flux matrix [kW/m] and (b.) power matrix [kW] for a moored point absorber (Babarit et al. 2012).	20
10	From Contardo et al. 2018: (a.) wave diagram, with contours showing power in [kW/m] (b.) Difference in vertical wave spectra between "upwave" and four different "downwave" locations due to WEC energy extraction (solid: instrument data, dashed: model predictions)	21
11	Point-absorber WECs currently deployed and/or in development, from left to right: Ocean Power Technologies' PowerBuoy3, Fred Olson Lifesaver, and Columbia Power Technologies' SeaRAY	21

1.0 Executive Summary

Marine renewable energy devices, such as wave energy converters or tidal turbines, not only have the potential to provide clean, reliable power to the grid but may also offer new opportunities for ocean exploration by providing power for oceanographic sensors where other sources cannot. However, an important consideration in making this vision a reality is understanding whether the marine energy devices may interfere with oceanographic measurements. Interference may occur through several pathways, including sound produced by the device and the motion of the device itself. In this report, we provide an overview of interference pathways and their implications before exploring two use cases for marine energy-powered ocean observing platforms: a tidal-powered passive acoustic monitoring system and wave-powered wave measurement buoys. For each use case, we review the relevant literature and underlying physics of the systems as they are relevant to the desired measurements before making recommendations for design of such systems.

2.0 Introduction & Background

Marine renewable energy (MRE) devices (e.g., tidal turbines, wave energy converters) introduce acoustic, kinetic, electrical, and/or magnetic noise or disturbance into the environment. When MRE devices are used to power co-located ocean instrumentation, these disturbances may interfere with end-use ocean observing objectives. This report seeks to better understand the effects of these disturbances and inform design considerations for such systems to avoid critical interference through the analysis of two specific case studies.

2.1 Overview of MRE Interference Mechanisms

Interference from MRE devices is possible through three pathways: electrical, acoustic, and kinetic (motion). In this section we will provide a brief introduction to each of these, before providing a more in depth investigation of specific use cases where acoustic and motion interference play a critical role in the subsequent chapters.

2.1.1 Electrical

Electrical interference with sensors is a common challenge in ocean instrumentation integration, and can affect all types of digital measurements. As an example, Malinka et al. 2018 used hydrophones integrated into the foundation of a full-scale tidal turbine to monitor harbor porpoise behavior at the deployment site. Electrical interference from an unknown source resulted in noise in the frequency band where harbor porpoises vocalize, significantly reducing the detection range of the passive acoustic monitoring system. Unfortunately, electrical interference is difficult to predict, but can be mitigated through good grounding practices and electrical isolation of components. Electrical interference pathways will also be highly specific to the device configuration and its electronics hardware. For this reason, we do not investigate electrical interference further in this report, but emphasize that it is an important consideration and requires testing before deployment.

2.1.2 Acoustic

All MRE devices will generate some sort of acoustic noise. This noise can come from two sources: mechanical or audible electrical noise (e.g., generators, bearings, switching of power electronics) and noise from induced turbulent flow. Acoustic measurements of MRE devices to date indicate that mechanical noise will typically be tonal or impulsive in nature. Interference from mechanical noise can, in many cases, be mitigated during design by avoiding non-critical moving components. For example, metal flaps designed to reduce silt inflow on the DeltaStream turbine created loud clanging noises, an issue which could likely have been mitigated in the design phase (Malinka et al. 2018). Similar sources of mechanical sound have been observed from wave energy converters.

Conversely, turbulent flow through turbines will generate acoustic noise that is typically broadband and continuous in nature (Lloyd, Turnock, and Humphrey 2014), and which may vary with the operating state of the MRE device (Polagye and Murphy 2015). Flow induced by wave interactions with wave energy converters will also produce broadband sound, though it will be less continuous in nature.

In addition to radiated sound, turbulence-induced pseudo-sound (“flow noise”) can occur when turbulent structures are advected over a hydrophone (e.g., hydrophone is stationary in a

turbulent flow, or moving in a stationary field). Flow noise will result in increased noise levels, though this is a factor for deployment of hydrophones in any tidal or wave-driven environment and not unique to MRE-powered systems.

Sound generated by MRE devices will most directly impact passive acoustic measurements, as it may mask detections of sounds of interest and reduce the effective range of monitoring capabilities. It also has the potential to affect active acoustic measurements if the MRE device produces sound at the operating frequency of the sensor (typically on the order of kHz or MHz). Finally, acoustic interference may indirectly affect any biological measurements if the MRE device is audible to the species of interest. However, it is important to consider audibility and possible behavioral changes in the context of other anthropogenic noise (e.g, vessel traffic, marine construction).

2.1.3 Motion

When oceanographic sensors are coupled with MRE devices, the motion of the MRE device may interfere with sensor operation. This is more likely to be a concern for wave energy converters (WECs) than for tidal turbines, because WECs are inherently coupled to wave motion. The challenges associated with interference due to WEC motion were evidenced by a 2018 demonstration project where an instrumentation system including hydrophones, optical cameras, and multibeam sonars was coupled with a point absorber-type WEC (Joslin et al. 2019). Entrained air from waves crashing on the hull of the WEC created bubbles that often obscured the field of view of both the optical cameras and multibeam sonars, and the heaving motion of the device created a challenge for target detection and tracking. For a floating tidal turbine platform, similar challenges can be expected, though the platform would likely be deployed in a location with less energetic wave conditions, so entrained air/bubbles may not be a significant concern. However, effects of turbulence and vibration at high current should be considered. For passive acoustic measurements, platform motion can result in flow noise when the hydrophone has significant velocity relative to the ambient water.

Motion may also interfere with measurements that rely on accelerometers or gyrometers, such as estimation of wave parameters. An appealing application for micro-scale wave power is to power wave buoys, as they are typically deployed in locations where there is a strong wave energy resource. However, the wave energy converter would not only respond differently to waves (e.g., be tuned to maximize its own velocity), but would also inherently alter the surrounding wavefield due to the extraction of energy.

2.2 Use Cases

In this report, we will investigate two use cases for marine energy-powered ocean observing platforms that provide insight into the role that both acoustic and motion interference may play. First, we investigate how acoustic interference may impact a tidal-powered passive acoustic monitoring system, then, we explore the implications of platform motion and energy extraction for a wave energy converter-powered wave measurement buoy. For both use cases, we review relevant literature and make recommendations for future system design.

3.0 Use Case 1: Tidal-powered Passive Acoustic Monitoring

Passive acoustic monitoring (PAM) is routinely used to monitor the presence of vocalizing marine species, anthropogenic noise pollution, and ambient sound levels in the marine environment (Howe et al. 2019). Many widely used PAM systems (e.g, Chelonia Ltd. C-POD; Multi Électronique AURAL-M2) are autonomous systems - power is provided by an onboard battery, and data or processed data products are only available after the recovery of the system. However, for many applications, it is desirable to have access to data in real-time or near real-time (Van Parijs et al. 2009). For example, during construction operations or vessel navigation, real-time information about marine mammal presence can be used to limit acoustic emissions or avoid collision. Cabled recording systems can meet this need - power and data transmission are facilitated by a cable to shore. However, such systems are expensive and require significant infrastructure development, and many operational systems in the US are operated by the navy, meaning that access to data is limited (Melinger et al. 2007; Van Parijs et al. 2009).

Recent developments in PAM technology have aimed to bridge this gap by providing data in real-time or near-real time via satellite connection. Baumgartner et al. 2019 developed a moored buoy system for real-time monitoring of baleen whales that is capable of 12+ month deployments. Briefly, the system consists of a mooring containing an acoustic monitoring system capable of real-time detection that is connected via a compliant cable to a surface expression that supports an Iridium satellite system. Calls are detected in real-time using a pitch-tracking approach to identify tonal calls, and classification uses quadratic discriminant analysis to compare detected calls to a library of known call types. Classification has varying accuracy for different species, but analysis showed that more than 25% of calls were missed for all whale species present (Right, Humpback, Sei, and Fin). Detected calls are transmitted to shore via satellite every two hours with data transmission rates selected to minimize satellite service costs. SMRU consulting¹ developed a lower cost real-time acoustic buoy (the Coastal Acoustic Buoy; CAB) for short-term deployments in coastal regions. On this system, hydrophones are integrated into the surface expression, eliminating the need for an expensive compliant cable. The CAB has an onboard computer that runs PAMGuard², an open-source software package for passive acoustic monitoring. Raw data are stored onboard while PAMGuard data products (e.g., average noise level, detection information) can be relayed in real-time over a 3G or radio connection. When data are processed and transmitted in real-time, deployment duration is limited to approximately 14 days. Finally, ongoing work at PacWAVE, a wave energy test site off the coast of Oregon, has led to the development of the Coastal Real-time Acoustic Buoy (CRAB), an autonomous real-time passive acoustic monitoring buoy that is similar in concept to the system presented in Baumgartner et al. 2019, except that data are transmitted to the surface using an acoustic modem rather than a flexible cable. Battery life is limited to 6 months, meaning that for permanent installations, regular maintenance will be necessary, and the current system calculates noise summary metrics, but does not currently support real-time classification of marine mammal vocalizations or other sounds.

While these systems all represent promising advances in autonomous, real-time passive acoustic monitoring technology, challenges related to data bandwidth, real-time computing, and deployment duration are ubiquitous. A possible solution is to power systems with the hydrokinetic energy available at the monitoring site using devices such as tidal turbines or wave energy converters. This would extend deployment durations, as monitoring equipment would only need to be serviced when equipment failed, and provide the additional power necessary for advanced onboard computing (e.g., deep learning). However, if such a system is to be

1. <http://www.smruconsulting.com/products-tools/cab/>

2. <https://www.pamguard.org/>

Turbine	Capacity	Measured Frequency Range	Tonal Sounds	Broadband Sound	Peak decidecade SL (dB re 1 μ Pa @ 1 m)	Peak decidecade bin (Hz)	Citation
Schottel	50 kW	20-40000	between 2000 and 400 Hz	to 20000 Hz	122	500	Schmitt et al. 2015
Open Hydro	2.2 MW	70-80000	between 20 and 1300 Hz	40 to 8000 Hz	152	128	Lossent et al. 2018
Atlantis AR1500	1.5 MW	10-40000	20,000 Hz (harmonics observed)	50 to 2000 Hz	143, 10+ dB lower in bands not containing tone*	100	Risch et al. 2020
RivGen	35 kW	50-1000	100 Hz (varied with turbine operational state)	50 to 1000 Hz	132, 10+ dB lower in bands not containing tone*	100	Polagye and Murphy 2015

*Risch 2020 and Polagye 2015 do not report source level. Risch 2020 reports the average noise level from drifting measurements 0-20 m from the turbine, and Polagye 2015 reports the noise level measured at the closest point of approach to the turbine during drifting measurements

Table 1. Overview of existing acoustic measurements of tidal turbines. To facilitate comparison, only studies that report sound in decidecade levels are included.

useful for passive acoustic monitoring, it is critical to understand and mitigate any acoustic interference from the marine energy device that may impact passive acoustic recordings. In the present work, we discuss important considerations in the design of such a system and assess the impacts of acoustic interference.

A tidal-powered passive acoustic monitoring system has been proposed for real-time monitoring of southern resident killer whales in Puget Sound to alert ferry operators to their presence and avoid potential collision. This system will expand the capabilities of the CRAB system to include real-time classification and longer deployment durations. Here, we use this proposed system as a case study to explore the anticipated characteristics of acoustic interference, practical limits for sound emissions from the marine energy converter, and implications of hydrophone placement relative to the turbine. First, we review existing knowledge surrounding the radiated acoustic noise generated by tidal turbines and the acoustic characteristics of southern resident killer whale vocalizations. This information is used to analyze the impact that radiated noise from a tidal turbine might have on the detection range of passive acoustic monitoring systems. Finally, we analyze the impact that changes in mean velocity and turbulent kinetic energy in turbine wakes might have on turbulence-induced pseudosound (“flow noise”) in the vicinity of the turbine, and implications for hydrophone placement. Our analysis is used to inform recommendations for design of tidal-powered passive acoustic monitoring systems. While monitoring of southern resident killer whales is used as a case study in this work, similar analysis could be extended to other species and the characteristics of most marine mammal vocalizations are relatively well documented.

3.1 Acoustic Emissions from Tidal Turbines

Studies of the acoustic emissions of tidal turbines and other marine energy converters have typically had the objective of understanding any effects they may have on marine life (e.g., hearing effects, behavioral changes) (Polagye and Bassett 2020). Here, we investigate this

topic with a different goal: understanding how sound emitted by a turbine may impact co-located passive acoustic monitoring.

Table 1 summarizes several published acoustic measurements of tidal turbines. Several other studies (e.g., Bevelhimer, Deng, and Scherelis 2016; Hastie et al. 2018) have analyzed or discussed acoustic emissions from tidal turbines, however, here we focus on those that report sound pressure level (SPL) in decidecade (third-octave) levels to facilitate comparison between studies. While the power output of a turbine used to power a passive acoustic monitoring system would likely be an order of magnitude smaller than the smallest turbine included in Table 1, these studies do provide valuable insight into the characteristics of sound emissions. All studies report both broadband (i.e., spans a wide range of frequencies) and tonal sounds (i.e., sound is concentrated over a narrow range of frequencies) associated with turbine operation. Broadband noise generally decreases in intensity with increasing frequency, with peak levels below 1000 Hz. Tonal sounds vary between turbines in both frequency and structure - tones were between 20 and 20,000 Hz, with or without harmonics, and some were frequency-modulated while others were relatively constant in frequency. Multiple studies (Polagye and Murphy 2015; Risch et al. 2020) hypothesize that observed tonal sounds were produced by the turbine generators, though this is difficult to verify. Polagye and Murphy 2015 found that acoustic emissions varied in both frequency content and intensity with turbine operational state. Finally, the limited data available indicate that sound levels generally decrease with turbine size, meaning that any turbine used to power a passive acoustic monitoring system would likely produce lower intensity sound than the turbines described here. However, our use-case application represents a stand-alone energy harvesting system for which all components will be submerged. A typical tidal turbine installation intended to provide power to the grid, like those measured in the aforementioned studies, would separate switching power electronics needed to control the turbine generator and condition its power from the turbine itself. Such components produce noise that varies with switching frequency and rotation rate³, and may contribute to acoustic emissions from a small turbine used to power in situ instrumentation.

In addition to field measurements, some efforts have been made to model the radiated sound generated by turbulent flow through tidal turbines. Li and Çalişal 2010 use a discrete vortex model (DVM-UBC) to model the performance of an axial-flow turbine, and then use a numerical model to calculate the wake-induced velocity. Results are nondimensionalized, but show peak acoustic intensity at 4 Hz followed by a roll-off in acoustic intensity with frequency. Lloyd, Turnock, and Humphrey 2014 used a large eddy simulation (LES) to model sound produced by a lab-scale turbine. The model was validated by comparing performance characteristics of the turbine with lab tests before scaling results to a full-scale turbine using the Strouhal number. Turbine sound intensity peaked at the blade passing frequency, with peak levels of 144 dB re 1 uPa, which is comparable to field measurements. A major limitation of these models is that they do not account for mechanical noise (i.e., tonal sounds), and therefore likely underestimate sound levels at some frequencies. However, paired hydrodynamic-acoustic models may prove a useful tool for estimating how turbine sound might change with tidal currents, and therefore how marine mammal detection capabilities might vary with turbine operating conditions.

Directionality of acoustic emissions may also be a consideration for placement of co-located hydrophones. While Lossent et al. 2018 did not find evidence of directionality in in situ measurements of a 2.2 MW turbine, modeling efforts by Li and Çalişal 2010 did indicate directionality in both the intensity and frequency content of sound produced by the turbine. Future measurements of turbines used to power passive acoustic monitoring systems should include measurements from multiple angles relative to the turbine to investigate whether

3. <https://support.industry.siemens.com/cs/document/83180185/engineering-manual-sinamics-g130-g150-s120-chassis-s120-cabinet-dti=0&lc=en-WW>

directionality should be considered in hydrophone placement.

3.2 Marine Mammal Vocalizations

In order to assess the impact that acoustic emissions from a tidal turbine would have on detection of marine mammal vocalizations, it is important to understand the acoustic characteristics of those vocalizations. Here, we focus on the vocalizations of orcas (*Orcinus orca*), and, because the characteristics of orca calls will vary between populations and social groups (pods) (Ford 1987), we specifically focus on southern resident killer whales (SRKW). However, literature on the characteristics of marine mammal vocalizations is abundant, and similar information is available for other populations/species.

Orcas produce three types of calls: echolocation clicks, whistles, and pulsed signals. Clicks are short ($<250 \mu\text{s}$), broadband (10-100 kHz) pulses used for echolocation (Ford 1987). Whistles are tonal signals with limited harmonics or sidebands that are typically observed when orcas are socializing, and vary widely in frequency content and structure (Ford 1987). Thomsen, Franck, and Ford 2001 found that resident killer whale whistles are frequency-modulated tones with an average bandwidth of 4.5 kHz and an average dominant frequency of 8.3 kHz, with an average duration of 1.8 seconds. While Thomsen, Franck, and Ford 2001 did not quantify the source level of whistles, they are qualitatively described as lower source level “short range” calls used when whales are in close proximity to one another. Pulsed signals are the most common and characteristic orca call, and are composed of pulses generated at high repetition rates (250-2000 pulses/second). Unlike whistles, pulsed signals are characterized by more complex structures with multiple harmonics. Pulsed signals usually fall between 1 and 6 kHz, though high-frequency components of the call may reach 30 kHz, and signals can last anywhere from 5 ms to 10 s, with the majority between 0.5 and 1.5 s (Ford 1987). Ford 1987 found that pulsed signals fell into distinct categories and the same calls were repeated by population groups over the course of a five year study. Twenty-six pulsed signal call types were associated with SRKWs, and, while most calls were shared by more than one pod, individual pods had specific variants of the calls (subtypes). Ford 1987 does not estimate source levels of pulsed signals, but does present detailed information about the frequency content of each pulsed call type. More recent studies have analyzed call source level. Holt et al. 2009 found that the peak root mean square (rms) source levels of SRKW calls ranged from 133-174 dB re 1 μPa at 1 m with a mean of 155 dB re 1 μPa , and found a positive correlation between background noise levels and call source level (e.g., whales increased their volume in louder conditions).

3.3 Passive acoustic monitoring ranges

The maximum range at which a marine mammal vocalization will be detectable will depend on the source level (intensity) of the call, the frequency content of the call, ambient or anthropogenic noise levels in the frequency band of the call, and the bathymetry of the region between the marine mammal and the hydrophone. In this section, we review two relevant PAM studies that analyzed detection range. Riera et al. 2019 performed passive acoustic monitoring of resident killer whales off of Vancouver Island - particularly relevant to the selected case study given the study population and location. Acoustic recordings were made using AURAL-M2 (Multi Électronique) autonomous recorders. Recorders were deployed for periods of several months and operated on approximately 33% duty cycles (10 minutes on; 20 minutes off). While it is not explicitly stated, data storage capacity appears to have limited deployment length/duty cycle volume rather than battery power. The maximum range at which orcas could be detected

was estimated using a ray-tracing model that incorporated site bathymetry and the recorded ambient noise levels. Orca calls were modeled with a source level of 152 dB re 1 μ Pa @ 1 m at 1200 Hz and a duration of 1 s. Ambient noise was averaged in 1-month bins to evaluate any seasonality. Due to variable bathymetry at the deployment site, the maximum range where an orca could be detected not only varied with ambient noise levels, but was also dependent on angle relative to the hydrophone. The maximum detection range was 8.8 km in July, while the minimum range was 3.5 km in January. Shorter time-scale variability in detection range due to anthropogenic noise (e.g., vessel passing) or tides (e.g., flow noise) is not analyzed.

Malinka et al. 2018 performed passive acoustic monitoring of harbor porpoises in Ramsey Sound, Wales. While harbor porpoises produce higher frequency (27-120 kHz) calls than orcas, this study is particularly relevant because hydrophones were integrated into the base of a 400 kW tidal turbine with the objective of understanding potential environmental impacts of the turbine. This study demonstrates some of the challenges associated with passive acoustic monitoring at highly-energetic tidal energy sites - five out of twelve deployed hydrophones failed after deployment, and there was persistent electrical noise in the same frequency band as porpoise vocalizations. The electrical noise masked click detection, and a longer detection range would likely have been possible if the electrical noise had been identified and mitigated prior to deployment. The authors use a simple propagation model to estimate detection range, defining the ambient noise level based on the electrical noise band. The estimated maximum detection range varied between 20 and 200 m depending on the source level of the call. The authors note that, because electrical noise dominated the frequency band of interest, detection capabilities did not vary significantly with turbine operational state or tidal current, but this would be a consideration for other similar studies.

While the higher frequency of harbor porpoise calls certainly plays a role, the orders-of-magnitude difference between the detection ranges in these two studies underscores the importance of understanding interference if tidal turbines are to be used to power passive acoustic monitoring systems. Therefore, in the next section, we explore the relationship between turbine-generated acoustic noise and detection range.

3.4 Detection range in the presence of a turbine

A simple propagation model is used to model the effects of turbine noise on marine mammal detection range. We note that a more complex model, such as the ray-tracing model used in Riera et al. 2019, would give more accurate results for a specific deployment scenario. However, a propagation model provides insight into permissible turbine noise levels for effective passive acoustic monitoring.

The received level (RL) of a marine mammal call at a hydrophone will be:

$$RL = SL_{call} - TL, \quad (1)$$

where SL_{call} is the source level of the call and TL is the transmission loss, and all terms are in dB re 1 μ Pa. Using a combined spherical/cylindrical propagation model to model transmission loss:

$$TL = 20 \log_{10}(d) + 10 \log_{10}(r) - 10 \log_{10} d + \alpha r, \quad (2)$$

where d is the water depth, in m; r is the range from the hydrophone, in m; and α is the frequency-dependent coefficient of attenuation, in dB/m (Francois and Garrison 1982a, 1982b).

The call can be considered detectable if it exceeds the noise level in the same frequency band by some threshold, T dB. Here, we use a threshold of $T = 5$ dB and estimate the noise level of the turbine at the hydrophone as:

$$NL = SL_{turb} - 20 \log_{10}(s) - \alpha s, \quad (3)$$

where SL_{turb} is the source level of the turbine and s is the separation distance between the turbine and the hydrophone, in m. This expression assumes spherical spreading between the turbine and the hydrophone. Equations 1, 2, and 3 can be combined to create an expression for the maximum turbine source level that will permit detection of the marine mammal call at a given range, r_{max} :

$$SL_{turb} < SL_{call} - 20 \log_{10}(r_{max}) - 10 \log_{10}(r_{max}) + 10 \log_{10}(d) - \alpha r_{max} + 20 \log_{10}(s) + T. \quad (4)$$

To explore the practical limits for turbine noise, we modeled a orca call at 1000 Hz with a source level of 152 dB (the same source level as in Riera et al. 2019), and estimated the maximum turbine noise level in the decidecade band containing that frequency (891-1122 Hz) as a function of r_{max} and s following Equation 4. To provide a more accurate estimate, we used the sound pressure level of the call by integrating over the decidecade band (156 dB re 1 μ Pa). Because the rate of attenuation increases with frequency, α was conservatively calculated at the upper end of the decidecade band (1122 Hz).

Figure 1 shows the maximum sound pressure level of the turbine in the 1000 kHz decidecade band as a function of turbine/hydrophone separation (s) and detection range (r_{max}). Due to the logarithmic nature of transmission loss, relatively small changes in the distance between the turbine and the hydrophone have a significant impact on acceptable turbine noise levels - for a maximum detection range of 500 m, moving the hydrophone from 1 to 3 m from the turbine results in a nearly 10 dB increase in the turbine noise limit. While this is a somewhat oversimplified model that does not account for bathymetry, changes in sound speed, or the wide variety of orca vocalizations, it does provide some insight into the feasibility of tidal-powered passive acoustic monitoring system. While most of the turbines described in Table 3.1 are louder than the thresholds in Figure 1, the sound levels from the 50 kW turbine in Schmitt et al. 2015 (the smallest turbine reported) in the 1000 Hz decidecade band would permit detection of orca calls to a range of approximately 2500 m when the hydrophone was 3 m from the turbine - a value comparable to the detection ranges calculated in Riera et al. 2019. We note that this model also does not account for ambient noise or other anthropogenic noise sources, and if these sources exceeded noise generated by the turbine, they would be the limiting factor for marine mammal detection rather than the noise generated by the turbine.

3.5 Turbulence-induced pseudosound

In addition to radiated sound, turbulence-induced pseudo-sound (“flow noise”) can occur when turbulent structures are advected over a hydrophone (e.g., hydrophone is stationary in a turbulent flow, or moving in a stationary field). Bassett et al. 2014 investigated flow noise at Admiralty Inlet in Puget Sound, WA and found that at peak tidal currents (≈ 1.8 m/s), noise levels below 50 Hz were over 40 dB higher than at mean slack tide. Flow noise levels increased with mean tidal velocity, and decreased with increasing frequency with a slope of approximately $f^{-3.2}$. While the impact of flow noise is an important consideration for low-frequency passive acoustic monitoring in any tidal or wave-dominated environment, energy extraction will change the characteristics of the flow (Chamorro et al. 2013; Guerra and Thomson 2019) and therefore alter the characteristics of observed flow noise. While flow noise is unlikely to affect measurements above 2 kHz even in the most extreme energetic conditions, it may impact recordings of low- or mid-frequency marine mammals, such as orcas, and is worth investigating.

Bassett et al. 2014 developed a flow noise model that utilizes measurements of velocity and turbulence. The flow-noise pressure spectrum, in dB, is given by:

$$S_p(f) = 10 \log_{10} \frac{a \rho^2 \epsilon^{2/3} \bar{u}^{8/3} f_{sh}^{23/15} f^{-16/5}}{(2\pi)^{2/3} 10^{-12}}, \quad (5)$$

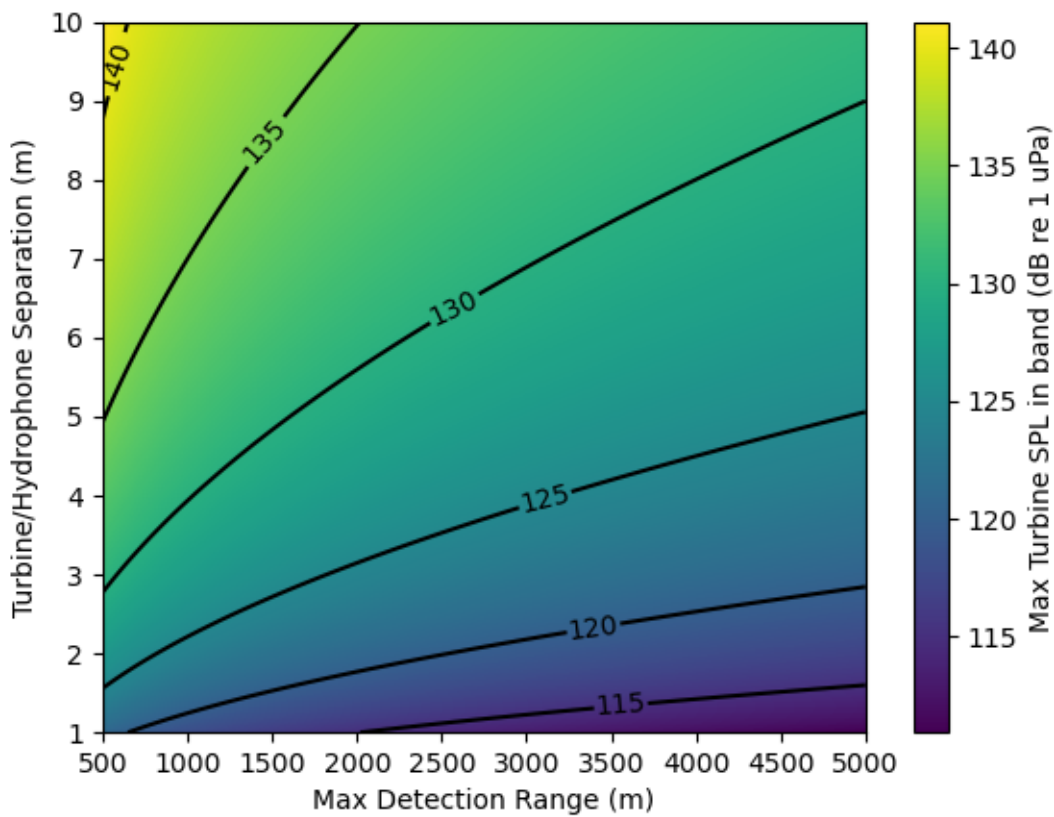


Figure 1. Maximum turbine SPL at 1 m in the 1 kHz decidecade band as a function of maximum orca detection range and separation distance between the turbine and the hydrophone. Note that where ambient noise levels exceed turbine noise, ambient noise will limit detection rather than turbine noise.

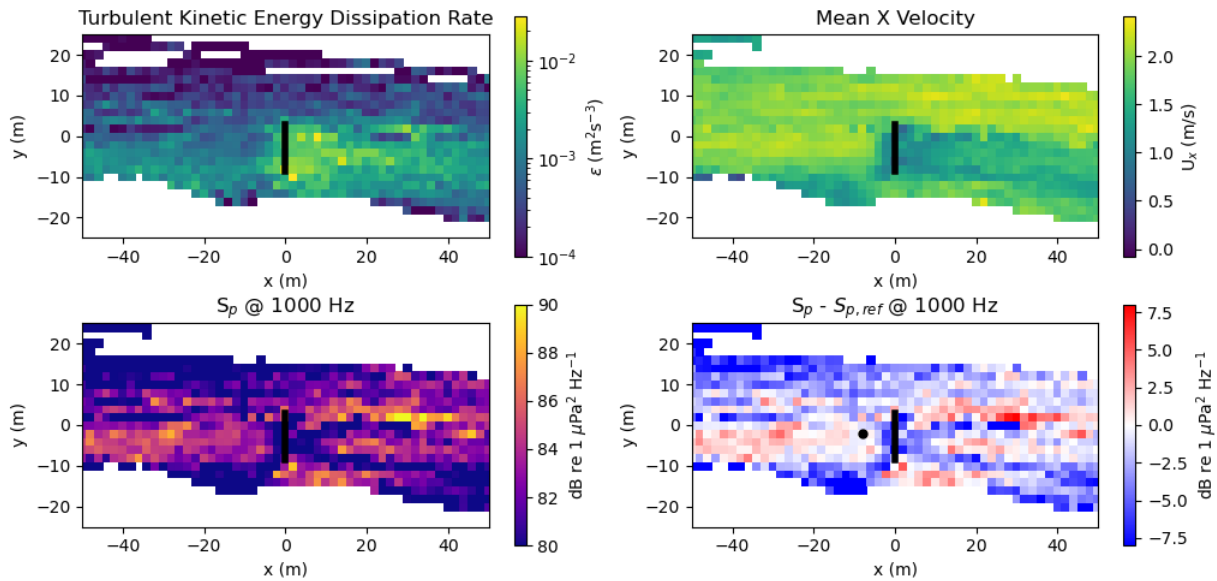


Figure 2. a) Turbulent kinetic energy dissipation ratio (ϵ) in the Kvichak river during operation of the RivGen turbine (from Thomson and Guerra 2018, b) mean horizontal velocity during operation of the RivGen turbine (from Thomson and Guerra 2018, c) estimated pressure spectra from flow noise at 1 kHz using Equation 5, and d) difference between the estimated pressure spectra and a reference point, indicated by the black dot.

where a is a constant; ϵ is the turbulent kinetic energy dissipation rate, in m^2s^{-3} ; \bar{u} is the mean flow velocity projected along the principal axis of the flow, in m/s; and f is the frequency, in Hz. The shoulder frequency, f_{sh} , is the transition frequency between two regimes - below f_{sh} , pressure fluctuations have much smaller length scales than the size of the hydrophone. Above f_{sh} , length scales are near or larger than the size of the hydrophone, and partial cancellation over the surface of the hydrophone occurs. Bassett et al. 2014 found empirically that the shoulder frequency was described by:

$$f_{sh} = 0.1 \left(\frac{\bar{u}}{d} \right), \tag{6}$$

where d is the characteristic size of the hydrophone (i.e. length of the hydrophone in the direction of the flow), in m. From Equation 5, it is clear that the magnitude of flow noise will increase with both ϵ and u . In the wake of a turbine, an increase in ϵ is expected, but also a decrease in the mean velocity, u , due to energy extraction (Guerra and Thomson 2019). To investigate the effect that this would have on a hydrophone within the wake of the turbine, we estimate flow noise levels using Equation 5 with turbulence measurements around the Ocean Renewable Power Company (ORPC) riverine turbine (RivGen) in the Kvichak river in Igigugig, Alaska (Thomson and Guerra 2018). Data collection methods can be found in Guerra and Thomson 2019. To provide a reasonable estimate, we used $a = 1.5$ and $d = 1.9$ cm. We note that this is the same turbine investigated in Polagye and Murphy 2015, though because Polagye and Murphy 2015 used drifting hydrophones any changes in measurements resulting from variable flow noise levels in the turbine wake would be minimal.

Figures 2a and 2b show ϵ and u measured while the turbine was operational, respectively (from Thomson and Guerra 2018), Figure 2c shows the estimated pressure level from

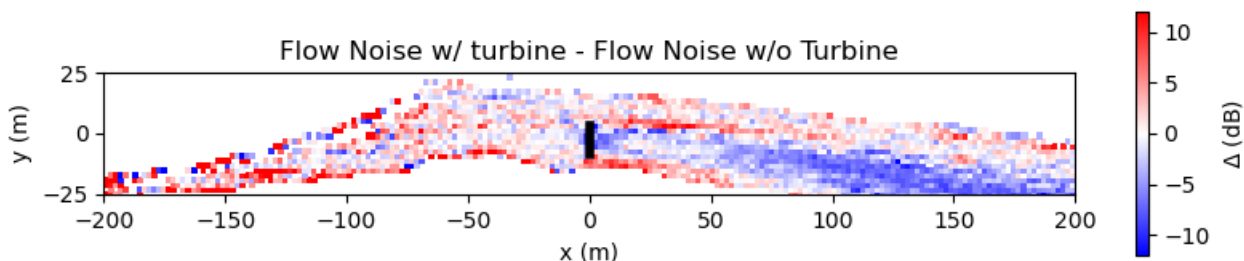


Figure 3. Estimated difference between flow noise in the Kvichak river at 1 kHz before installation of the RivGen turbine and while the turbine was operational, using data from Thomson and Guerra 2018

flow-noise at 1 kHz (from Equation 5), and Figure 2d shows the relative difference between the estimated flow noise at 1 kHz and a point upstream of the turbine. Figure 3 shows the difference in flow noise levels calculated using flow measurements made before the turbine was installed and after the turbine was installed and operational. While the measured turbine is significantly larger (35 kW) than would be necessary to power a passive acoustic monitoring system, it offers some insight into trends in flow noise around a tidal turbine. While the data are relatively noisy, it is clear that the decreased velocity in the turbine wake results in a decrease in flow noise despite elevated turbulent kinetic energy dissipation rates. Conversely, in the bypass flow (i.e., region of the flow downstream of the turbine, outside of the wake), increased mean flow speeds result in an increase in flow noise levels. In a more hydrodynamically complex tidal environment, the magnitude of flow noise will change over time with tidal current velocity regardless of the presence of the turbine. The direction of the flow will also change with ebb and flood tide, meaning that if a hydrophone is in the turbine wake it will measure different levels of flow noise at the same mean tidal velocity during ebb or flood tide. This should be considered in determining the optimal placement of a hydrophone within the flow. We also note that the high-resolution wake characterization in Guerra and Thomson 2019 was performed using drifting instrumentation. Because the turbine was deployed in a river, the authors were able to make an assumption that the flow field was stationary in time and make measurements over the course of many hours or days. In a tidal environment, this resolution of in situ wake measurements at a single current velocity would not be possible. In practice, a combination of modeling, laboratory testing, and in situ point measurements would be necessary to characterize a tidal turbine wake.

3.6 Discussion and Recommendations

In this work, we have shown that while acoustic interference is an important consideration for the design of a tidal-powered passive acoustic monitoring system, it is not a critical problem that will prevent the successful development of such such systems. Based on the review and analysis in this document, we can make the following recommendations for design of a tidal-powered passive acoustic monitoring system:

- Review literature on vocalizations of the marine mammals of interest to identify the frequencies where calls will be detected early in the design process
- Turbine noise in the frequency band(s) where marine mammals of interest are vocalizing

should be well-characterized, including any directionality (e.g., detection range is higher/lower depending on position relative to the turbine)

- Mechanical noise from generators or other components should be minimized, especially in the frequency bands of interest. This could be considered in component selection (e.g., avoid a generator that produces tonal sound at frequencies of interest)
- When possible, maximize separation distance between the hydrophone and the turbine to reduce received levels of turbine noise at the hydrophone
- Turbine wakes affect the turbulent kinetic energy and mean flow velocity, which results in altered flow noise levels around the turbine. This may result in a net reduction or increase in flow noise levels depending on the position of the hydrophone relative to the turbine. This should be considered in hydrophone placement and data interpretation, especially in tidal environments where it will affect both sides of the turbine separately during ebb and flood tides.
- Deployment locations with strong horizontal gradients in tidal current velocity may prove ideal if it is possible to have the turbine in strong flow and the hydrophone in weaker flow to minimize flow noise.

We have also identified the following knowledge gaps which could be addressed through future research:

- There are no published measurements of the acoustic characteristics of micro-scale turbines, or turbine implementations including a full complement of power electronics and these data are needed to quantify detection ranges of tidal-powered passive acoustic monitoring systems.
- Turbine noise levels, and therefore detection range, will vary with tidal current speed/turbine operational state. This should be a focus of any field measurements.
- Directionality of sound produced by tidal turbines is also relatively poorly studied, and may have an impact on optimal hydrophone placement. Therefore, future field measurements should record turbine sound at multiple angles relative to the turbine.
- An understanding of the characteristics and extent of wakes from micro-scale turbines will facilitate an understanding of impacts on flow-noise for co-located passive acoustic monitoring systems.

In sum, tidal-powered passive acoustic monitoring appears to be feasible from an acoustic standpoint. However, successful development will require consideration of acoustic emissions throughout the design process.

4.0 Use Case 2: Wave-powered measurements of wavefields

4.1 Introduction

Measuring wavefields is critical for understanding pelagic and coastal system dynamics and comprehensive marine/coastal engineering design. Wave energy converters (WECs) provide an obvious source of energy for wave-measuring instruments, yet they create the nontrivial issue of altering the wavefield such instruments are measuring. While ocean waves can be measured from a variety of devices, e.g. pressure sensor arrays, buoy platforms, acoustic Doppler instruments, and X-band radar, this review will focus on modern low-power options including buoys and active acoustic instruments. There are two possible configurations to power a wave-measuring platform using WECs considered here. The first, and the simplest option, is to include the sensor package on the WEC body itself, assuming the WEC is a surface-following system. The second is to power a wave instrument (buoy, acoustic surface tracking (AST) capable instrument, pressure sensor array) using a WEC that is not physically coupled to the wave instrument. This configuration doesn't require the WEC to be a surface device.

In this chapter, we will provide an overview of how existing wave buoys function, how WECs extract energy from waves, and considerations for their combination.

4.2 Field Measurements of Ocean Waves

There are two methodologies to measure wave height, period, and direction from buoys: 1.) vertical acceleration in conjunction with wave slope and 2.) 3D particle motion (wave orbital velocity). Inertial measurement units (IMUs), or some combination of accelerometer-gyroscope-magnetometer, can be used to directly measure these properties. Herbers et al. 2012 found that GPS units could be used to directly measure horizontal and vertical displacements instead of an IMU, though an accelerometer is useful in place of low-accuracy vertical GPS data (Pearman et al. 2014, Thomson et al. 2018). In deep water, horizontal motion, measured by either GPS or IMU, can be used to estimate the vertical (Herbers et al. 2012). For wave measurements, deep water is defined as the depth where $\text{depth} > \text{wavelength}/2$. This is commonly referred to as "the deep water assumption."

Raw wave data are typically processed using spectral analysis. Wave energy, significant height and period can be found from the vertical autospectra alone, while wave direction and spread are calculated from the auto- and cross-spectra in the horizontal directions (Longuet-Higgins, Cartwright, and Smith 1963, Kuik, Vledder, and L.H.Holthuijsen 1988). Herbers et al. 2012, Thomson et al. 2018, and Rabault et al. 2020 provide helpful explanations of these equations, which are detailed below.

Wave energy spectra are often calculated using the Welch method: applying a Hanning or Hamming window on detrended samples of length X with 50% overlap and subsequently computing a discrete Fourier transform on the samples. Vertical spectra (S_{zz}) are typically calculated from vertical velocity (m/s), which is found from raw accelerometer or GPS data; horizontal spectra (S_{xx}, S_{yy}) are typically calculated using horizontal velocity (m/s) found from GPS speed over ground, horizontal displacement (m), or, for older wave buoys, pitch and roll.

Calculating significant wave height only requires the use of vertical measurements. Raw accelerometer data requires filtering, typically with a high-pass filter to remove low-frequency drift, and is integrated and smoothed with an RC filter either once or twice to solve for vertical velocity and displacement, respectively (Thomson et al. 2018). Corrections should be applied first if the sensor suite was not located at the buoy's center of mass. If the deep water assumption is applicable and the vertical data is not of sufficient quality, the vertical spectra can

be found from the horizontal components of motion, which have greater precision on GPS:

$$S_{zz} = S_{xx} + S_{yy} \quad (7)$$

The energy spectrum then, if using vertical displacement,

$$E(f) = S_{zz}(f) \quad (8)$$

And if using vertical velocity,

$$E(f) = \frac{S_{zz}(f)}{(2\pi f)^2} \quad (9)$$

Where f is wave frequency vector of S_{zz} . Peak wave period (T_p) is the inverse of f . Significant wave height (H_s) and the average wave period (T_m) are found from the first two spectral moments:

$$m_0 = \int_a^b E(f)df \quad (10)$$

$$m_1 = \int_a^b fE(f)df \quad (11)$$

Where a and b are the frequency limits, where a is typically no smaller than 0.0455 Hz and b is usually not greater than 1.0 Hz, depending on device sensitivity.

$$H_s = 4\sqrt{m_0} \quad (12)$$

$$T_m = m_0/m_1 \quad (13)$$

Following the derivation in Thomson et al. 2018, directionality can be calculated using the horizontal spectra (S_{xx}, S_{yy}) as defined previously and the cross spectra (C_{xy}, C_{xz} and C_{yz}). The cross spectra here refers to solely the real part of C_{xy}, C_{xz} and C_{yz} , which are complex numbers. These parameters are used to calculate the first two moments of the directionality spectrum, a and b , which in turn can be used to estimate wave direction. The same equations apply here regardless of the units that the data was measured in (units cancel out), and accuracy and precision depend primarily on sensor quality and platform design.

$$a_1(f) = \frac{C_{zx}}{\sqrt{(S_{xx} + S_{yy}) * S_{zz}}} \quad (14)$$

$$b_1(f) = \frac{C_{zy}}{\sqrt{(S_{xx} + S_{yy}) * S_{zz}}} \quad (15)$$

$$a_2(f) = \frac{S_{xx} - S_{yy}}{S_{xx} + S_{yy}} \quad (16)$$

$$b_2(f) = \frac{2C_{xy}}{S_{xx} + S_{yy}} \quad (17)$$

Wave direction, θ , is then:

$$\tan(\theta_1(f)) = b_1/a_1, \quad (18)$$

$$\tan(2\theta_2(f)) = b_2/a_2 \quad (19)$$

where θ is real (not complex) and in radians measured counterclockwise from East. If an IMU is being used, this may require correction with the local magnetic declination. Wave spread, ϕ , is

$$\phi_1(f) = \sqrt{2(1 - \sqrt{a_1^2 + b_1^2})}, \tag{20}$$

$$\phi_2(f) = \sqrt{\frac{1}{2} - \frac{1}{2}(a_2 \cos(2\theta_2) + b_2 \cos(2\theta_2))} \tag{21}$$

where ϕ is in radians. Note that there is a second formulation of these equations that only provides results in two quadrants, resulting in ambiguity in the result. However, as the second formulation does not require vertical acceleration data, it may be useful in coastal environments where the wave direction is relatively unidirectional if vertical acceleration data are not available.

The viability of wave data can be verified in two ways. One is the ability of buoy measurements to show characteristic f^{-4} dependence along equilibrium frequencies in the calculated vertical spectra (e.g. Pearman et al. 2014, Thomson et al. 2015), as shown in Figure 4, though this method fails in changing wind (‘forcing’) conditions (Thomson et al. 2013).

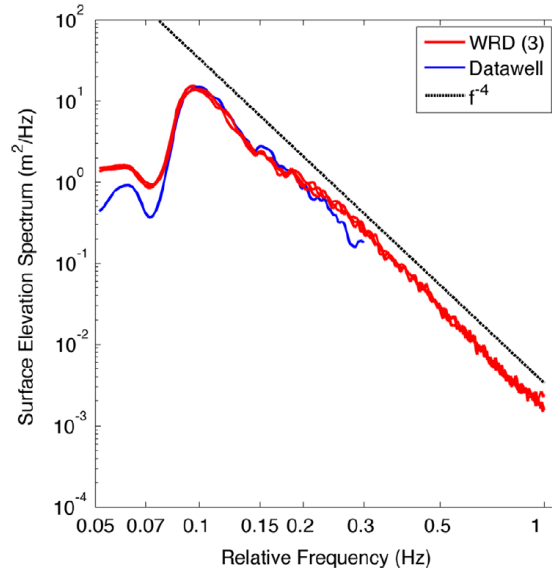


Figure 4. Data comparison between a commercial Waverider buoy’s and a custom-built drifter buoy’s vertical spectra, showing the characteristic f^{-4} slope (Pearman et al. 2014)

The second is a quality flag based on particle orbital motion as described by linear wave theory. For a given wave, the ratio of horizontal to vertical displacement spectra shouldn’t be greater than unity ($(S_{xx} + S_{yy})/S_{zz} \leq 1$, Figure 5). In deep water, this ratio should be 1 (e.g. Thomson et al. 2015, Rabault et al. 2020).

The accuracy of wave buoy measurement techniques was verified by O’Reilly et al. 1996 by testing a buoy operated by the NOAA National Data Buoy Center (NDBC) and a commercially available Datawell Waverider (DWR) buoy (Figure 6) against a pressure sensor array. An array of pressure sensors can measure wave parameters within the bounds of linear wave theory, which was found, for this particular array, to between 0.06 and 0.14 Hz with an error of “a few” percent as compared to linear wave theory. Compared to the pressure array, the DWR was biased < 1% high in wave energy, with an rms error of 5 degrees and 7% for wave direction

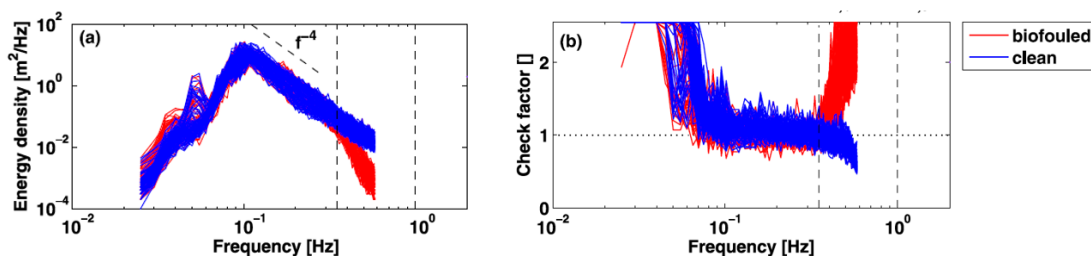


Figure 5. f^{-4} dependence and “check factor” quality control check. Bad data is where the check factor is greater than 1. (Thomson et al. 2015)



Figure 6. Commercial Datawell wave buoys (Herbers et al. 2012)

and spread, respectively. Since this study, most wave measurement platforms are tested against DWRs.

Bender et al. 2010 found that the standard error of a buoy using a simple GPS or IMU sensor package is around 5% if 3-axis accelerometer data isn't used to correct for gravity in steep wave slope situations (> 10 degrees). Standard error was seen to increase to 40% in hurricane-generated wavefields. Noise filtering of raw accelerometer data is also a critical step to ensure data quality (Bender et al. 2010, Thomson et al. 2018).

Commercially available wave buoys are generally not capable of measuring waves with periods smaller than 3 seconds ($f > 0.3$ Hz) because of size (commercial Datawell or NDBC buoys) or cost (as in Kohout et al. 2015 & Rabault et al. 2020). Smaller, research-developed units (Thomson 2012, Pearman et al. 2014) can measure down to 1 second wave periods. To measure waves, a buoy must be small enough relative to the wavelength that the wave energy passes through the buoy; there comes a point in decreasing wavelength where waves will begin to diffract around it. At the other end of the spectrum, because they are Lagrangian drifters, buoys cannot measure waves within the infra-gravity swell band (> 22 s) accurately (Herbers and Janssen 2016). Finally, because design and analysis are based around linear wave theory, instruments have difficulty measuring nonlinear wave dynamics, e.g. wave slapping/slamming, whitecapping and wave breaking. Examples of mooring configurations for commercial buoys can be found in Figure 7.

A buoy's ability to measure waves also depends on its wave-following ability, which in turn depends on the platform design. Spherical hulls (e.g. DWRs) have been shown to do this well (O'Reilly et al. 1996), though other buoy designs can achieve statistically accurate results with post-processing adjustment. NDBC buoys utilize a transfer function to correct platform wave

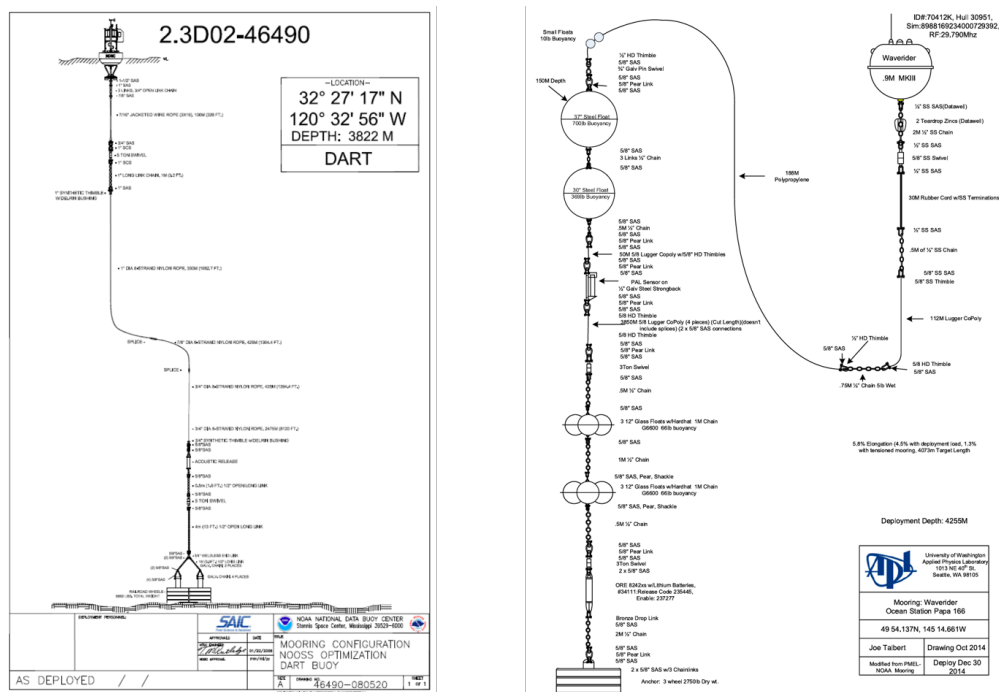


Figure 7. Buoy mooring diagrams (a.) NDBC DART buoy mooring (Teng 2002) (b.) Datowell buoy mooring (Thomson et al. 2013).

damping based on empirical data (Teng 2002). Quasi-Lagrangian platforms (e.g. Thomson et al. 2018) require post-processing due to damping (or acceleration) from platform restriction or locomotion. A wave buoy ideally won't have a natural frequency motion that creates peaks in wave spectral data, though Thomson 2012 inadvertently discovered that a buoy's bobbing motion didn't have an effect on the platform's ability to follow wave orbital motion in the horizontal plane. The vertical bobbing motion in this case was at a frequency higher than 1 Hz.

Another technique to measure waves is using acoustic surface tracking (AST). AST uses Doppler measurement techniques: an active acoustic signal is used to detect the air-water interface from below. A vertical beam measures the change in sea surface level, while 3 angled beams measure horizontal wave velocity. Waves measurable by this technique are limited by sampling frequency (Nyquist limit) and instrument depth (due to beam width and spread) (Pedersen and Lohrmann 2004). While quantitative values are not given, qualitatively, Pedersen and Lohrmann 2004 found that an acoustic instrument measured wave heights well but had high uncertainty in wave direction during storm events compared to a DWR. Analysis of AST data is done via the SUV method ('S' for surface, and 'U','V' referring to the horizontal components of the velocity vector) (Pedersen, Siegel, and Wood 2007), which is closely related to the traditional buoy methods outlined in this section.

4.3 Interference from Wave Energy Converters

4.3.1 WEC-influenced Wavefields

Energy harvesting is the critical interference issue with using WECs, regardless of design, to power wave measurement systems because energy extraction directly affects wave height. Wave energy is "stored" in a wave's height, and the power delivered by a wave depends on its



Figure 8. Nortek AWAC mounted in a bottom lander & a Datawell Waverider buoy (Pedersen and Lohrmann 2004)

significant height, H_s and energy period, T_e .

$$E = \frac{\rho g H_s^2}{16} \quad (22)$$

The wave energy flux per unit of wave crest length, P , in W/m, is given by:

$$P = \frac{\rho g^2 H_s^2 T_e}{64\pi}, \quad (23)$$

where g is the acceleration due to gravity, in m/s^2 , and ρ is the density of seawater, in kg/m^3 . Energy extraction therefore decreases wave height, and the distance and spread of the “downwave” decrease in wave height depends on the device’s size, type and PTO. Wave energy periods are not affected.

WECs are designed to harvest energy most efficiently from a particular range of wave periods. The waves that a device extracts energy from are characterized using a power matrix, which is found by multiplying a device’s capture width matrix by a wave energy flux matrix of a particular area of interest (Babarit et al. 2012), shown in Figures 9 and 10a. Capture width is the ratio of the power captured by a particular WEC design to the amount of power contained in the wave moving through it. The capture width matrix displays a device’s capture width under a variety of wave heights and periods and is developed from modeling and/or wave tank experiments (e.g. Bosma et al. 2015). A wave energy flux matrix, or a wave statistics diagram, displays the distribution of significant wave height and peak period of given area’s sea state, and is displayed as a percent or in units of kW/m. Power absorption largely depends on the device’s physical size, PTO tuning and the sea states it is deployed into (Babarit et al. 2012), (Contardo et al. 2018). Understanding these sea states is especially critical to the WEC’s performance because wave type, direction, spread, and variability all play into extraction efficiency and power production (Kerbiou et al. 2007, Saulnier et al. 2011, De Andrés et al. 2015). Subsequently, the degree to which a WEC affects a wavefield is proportional to both its size and efficiency in energy extraction.

The majority of wave energy studies to date have been building and improving fast numerical models, though computational fluid dynamics (CFD) simulations are run if greater detail is required. A comprehensive review of modeling techniques and studies are provided in Wolgamot and Fitzgerald 2015 and Windt, Davidson, and Ringwood 2018. Lab experiments in

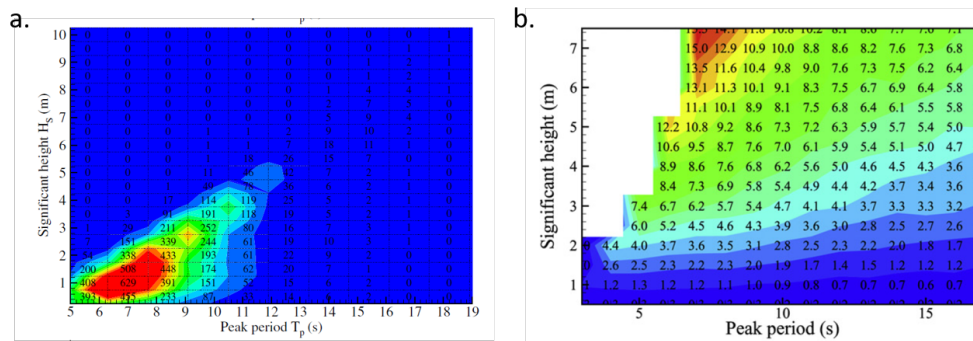


Figure 9. (a.) An example wave energy flux matrix [kW/m^2] and (b.) power matrix [kW] for a moored point absorber (Babarit et al. 2012).

wave tanks step up from models to prototypes and utilize scaled devices based on Froude number and contain some sort of PTO emulation (e.g. Stratigaki et al. 2014, Bosma et al. 2015, Bosma et al. 2020, Giassi et al. 2020). The effects of energy extraction on a wavefield has only been studied in-situ by Contardo et al. 2018 at the time of writing.

Several studies have investigated the effects of energy extraction on the surrounding wavefield. To date, most have been numerical, and have shown that the greatest reduction in wave height occurs in a spread behind the WEC or WEC farm, where reduction decreases with distance as the wavefield recovers. In one SNL-SWAN modeling study, 2 kW to 225 kW-capable WEC farms reduced waves heights from 2% - 25% in the immediate vicinity behind the farms (Chang et al. 2016). In Stratigaki et al. 2014, a prototype WEC farm is shown to reduce wave heights at a greater spatial scale under short-crested wave conditions than in long-crested waves, with up to 18% reduction of wave height in both cases. The effects of energy extraction on a wavefield have only been studied in-situ by Contardo et al. 2018 at the time of writing. In this study, Nortek AWAC ADCPs are used to measure the difference in wave height and spectra of incoming and outgoing waves from a trio of submerged, moored point-absorbers, each with a capacity of 240 kW. They found that wave heights decreased “downwave” if that particular wave frequency was harvested by the device, at reduction rates of 20%, 12%, and 9% at locations 40, 80, and 100 m downwave (not directly in line). Outside the lee of the WECs, effects weren’t measurable by an ADCP at 90 m distance. The downwave measurements were ground-truthed against a single ADCP “upwave” of the WECs. Wave height differences were not solely due to natural variation, though the WECs under study had an effect on par with natural landforms in the same area. They do make the assumption that the upwave AWAC is unaffected by the array.

While the primary destruction of wave height occurs behind WECs, incoming waves face out-of-phase waves radiated from the devices due to energy extraction (Babarit 2013, Yu and Li 2013). These radiated waves become important in designing WEC farms for optimum power harvesting Stratigaki et al. 2014, and are apparent in CFD simulations, as can be seen in Yu and Li 2013 for a floating two-body point absorber and in Cheng et al. 2021 for an oscillating wave surge converter.

4.3.2 Point Absorber Wave Measurements

Point absorber-type wave energy converters, like those shown in Figure 11, are the most likely candidates for power wave measurements given their surface-following characteristics. The two main types of point-absorbers in consideration are moored and two-body designs. Neither

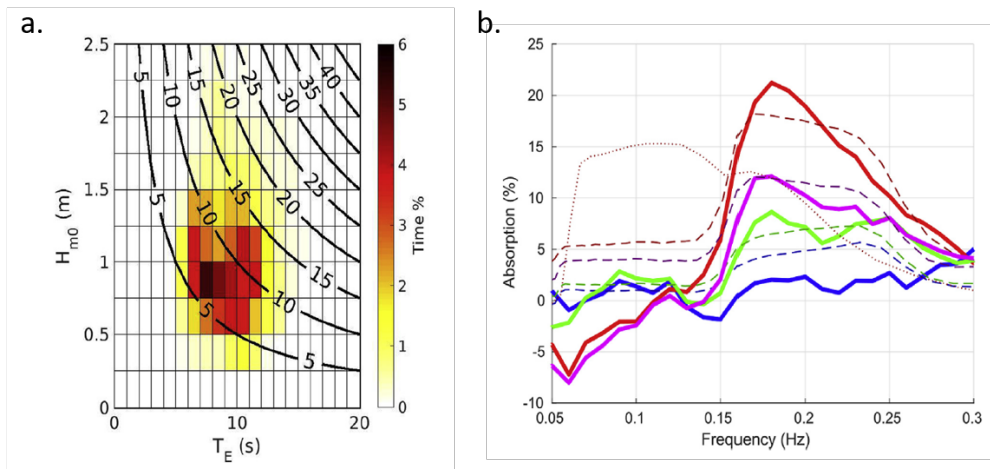


Figure 10. From Contardo et al. 2018: (a.) wave diagram, with contours showing power in [kW/m] (b.) Difference in vertical wave spectra between “upwave” and four different “downwave” locations due to WEC energy extraction (solid: instrument data, dashed: model predictions)

design responds to waves with energy periods below their natural frequency, each extracts the most energy when at resonance, and the moored type extracts more energy above its resonant frequency than the two-body floating design (Babarit et al. 2012, De Andrés et al. 2015). The former is a good wave follower in heave above its natural frequency, whereas the latter’s heave response changes with wave period and based on the PTO tuning (Yu and Li 2013). The 2-body system is a good wave follower in energy periods “sufficiently longer” than the resonant period, though there is a phase difference that increases when the wave energy period approaches the device’s resonant period. At resonance, there exists a maximum phase difference between the float and heave plate in the 2-body system, which then decreases with increasing wave period. As the PTO damping is increased (i.e. tuned to extract more energy from incoming waves), the relative motion between the two bodies decreases, which in turn increases the magnitude of heave response. Yu and Li 2013 also note that viscous drag was the primary damping force on the heave plate.



Figure 11. Point-absorber WECs currently deployed and/or in development, from left to right: Ocean Power Technologies’ PowerBuoy3, Fred Olson Lifesaver, and Columbia Power Technologies’ SeaRAY

Following the sum of the forces used for WEC analysis (Babarit et al. 2012), (So

et al. 2017),

$$m\ddot{X} = F_{ext} + F_{rad} + F_{PTO} + F_v + F_B, \quad (24)$$

a single wave-measuring/extracting system's motion is defined based on the system's wave excitation F_{ext} and radiation F_{rad} (wave-following ability), PTO response F_{PTO} , viscous damping due to taut mooring lines or heave plate hydrodynamics F_v , and gravity-buoyancy restoration forces F_B . The difference between this equation of motion for a floating WEC and a wave buoy is the addition of the PTO response (F_{PTO}) and viscous damping (F_v) terms. Viscous damping is typically neglected for wave buoys since damping from whitecapping and other sources is difficult to quantify.

According to linear wave theory, if a floating body is a perfect wave follower, the wave diffraction and radiation forces on and from that floating body cancel each other out. This isn't necessarily true when nonlinear hydrodynamics are in play, inducing viscous losses, though both WECs and wave buoys contend with this real-world issue. The PTO is capable of altering the buoy's response based on its control characteristics/tuning and efficiency.

When considering wave measurement instrumentation directly mounted to a wave energy converter, a point absorber's PTO response is the largest road block to accurate wave-following aside from buoy hull design. Because they are typically designed to resonate at a natural frequency corresponding to a particular wave period, point absorbers naturally have a lower (damped) response at other frequencies. Both a change in amplitude and a phase difference then exist between wave and device motion, and this response behavior induces hydrodynamic viscous losses. (Wolgamot and Fitzgerald 2015). Because it is a mechanical system, viscous losses from friction and other inefficiencies reduce the PTO response and hence the devices wave-following ability.

The addition of a heave plate creates another source of damping in vertical wave-following ability (Yu and Li 2013). If the WEC is located in deep water, horizontal motion could be used to calculate the vertical motion and circumvent this problem, as in Equation 7 (Herbers et al. 2012), and similar to Thomson et al. 2018. Part of Thomson et al. 2018 studied the wave-measuring ability of a Wave Glider, an autonomous surface vehicle. Wave Gliders are cabled to an finned undersea module for locomotion - wave motion passively angles the module's fins, which create motion forward and dampens motion backwards. A heave plate would effectively damp motion in all directions, to varying degree. They then analyze and utilize a number of methods to correct the Wave Glider data, and observe a worse-case uncertainty in significant wave height of +/-5% (about 30 cm), an energy-weighted wave period error of +/-5%, and bias (RMS) errors up to 34 degrees in wave direction.

Horizontal motion will be damped by taut mooring lines and/or a 2-body point-absorber's heave plate, as mentioned above. Traditional wave buoys are moored to the seafloor, but allow slack for a drift circle of a specified radius (O 10-100 m). Motion limitation beyond the drift circle can show up in the wave data, usually as a "bump" in the spectral data at 30-35 s periods.

4.4 Discussion and Recommendations

In this chapter, we have reviewed how measurements are made from wave buoys and how they may be impacted by wave energy extraction. From this information, we can draw several conclusions about wave-powered wave measurements:

- WECs decrease wave heights of waves whose energy periods lie within the devices' response frequency range downwave of the devices. The efficiency of energy extraction depends on how well the WEC is tuned to the sea state it's deployed in, found by comparing the power matrix of a device to the total power contained in a wavefield.

- To power independent wave-measuring instruments using WEC-generated energy, the main concern is deployment location. If the sea states and their variability are known, it appears to be as simple as locating the instruments in the area upwave of the WEC(s), though it should be far enough that the waves radiated from the device damp out. In the wavefield behind the buoy, downwave effects are apparent in a spread in lee of the device up to a certain distance. The more energy a device extracts, the stronger this downwave “wake”.
- Measuring waves from a single point-absorber platform (either moored or floating 2-body) is more difficult. In both cases, it is not possible to measure waves with frequencies higher than that of the device’s designed natural frequency.
 - A moored point-absorber follows heave well in waves with frequencies below its natural frequency, though is most likely limited in measuring horizontal displacements because of the required taut mooring line. It is unknown how well it can measure wave slopes.
 - A floating 2-body point-absorber doesn’t particularly follow waves, but it rather reacts to them, which can result in motion greater or less than the original forcing wave. These devices do become wave followers in longer wave periods, when the relative motion between the 2 bodies approaches zero. Both the float–wave interaction and PTO–heave plate reaction alter the device’s heave-following ability and the magnitude of heave response. Due to hydrodynamic drag, the heave plate resists all motion, though it could be possible to use device’s horizontal displacements to correct vertical, after heave-plate resistance is corrected for.

References

- Babarit, Aurélien. 2013. "On the park effect in arrays of oscillating wave energy converters." *Renewable Energy* 58:68–78.
- Babarit, Aurélien, Jorgen Hals, Made Jaya Muliawan, Adi Kurniawan, Torgeir Moan, and Jorgen Krokstad. 2012. "Numerical benchmarking study of a selection of wave energy converters." *Renewable energy* 41:44–63. <https://doi.org/10.1016/j.renene.2011.10.002>.
- Bassett, C., J. Thomson, P.H. Dahl, and B. Polagye. 2014. "Flow-noise and turbulence in two tidal channels." *The Journal of the Acoustical Society of America* 135 (4): 1764–1774. <https://doi.org/10.1121/1.4867360>.
- Baumgartner, M., J. Bonnell, S.M. Van Parijs, P.J. Corkeron, C. Hotchkin, K. Ball, L. Pelletier, et al. 2019. "Persistent near real-time passive acoustic monitoring for baleen whales from a moored buoy: System description and evaluation." *Methods in Ecology and Evolution* 10 (9): 1476–1489. <https://doi.org/10.1111/2041-210X.13244>.
- Bender, L.C., N.L. Guinasso Jr., J.N. Walpert, and S.D. Howden. 2010. "A Comparison of Methods for Determining Significant Wave Heights - Applied to a 3-m Discus Buoy during Hurricane Katrina." *Journal of Atmospheric and Oceanic Technology* 27:1012–1028. <https://doi.org/10.1175/2010JTECHO724.1>.
- Bevelhimer, M.S., Z.D. Deng, and C. Scherelis. 2016. "Characterizing large river sounds: Providing context for understanding the environmental effects of noise produced by hydrokinetic turbines." *The Journal of the Acoustical Society of America* 139 (1): 85–92. <https://doi.org/10.1121/1.4939120>.
- Bosma, Bret, Ted Brekken, Pedro Lomonaco, Bryony DuPont, Chris Sharp, and Belinda Batten. 2020. "Array modeling and testing of fixed OWC type Wave Energy Converters." *International Marine Energy Journal* 3 (3): 137–143.
- Bosma, Bret, Tim Lewis, Ted Brekken, and Annette Von Jouanne. 2015. "Wave tank testing and model validation of an autonomous wave energy converter." *Energies* 8 (8): 8857–8872.
- Chamorro, L.P., C. Hill, S. Morton, C. Ellis, R.E.A. Arndt, and F. Sotiropoulos. 2013. "On the interaction between a turbulent open channel flow and an axial-flow turbine." *Journal of Fluid Mechanics* 716:658–670. <https://doi.org/10.1017/jfm.2012.571>.
- Chang, G, K Ruehl, CA Jones, J Roberts, and C Chartrand. 2016. "Numerical modeling of the effects of wave energy converter characteristics on nearshore wave conditions." *Renewable Energy* 89:636–648. <https://doi.org/10.1016/j.renene.2015.12.048>.
- Cheng, Yong, Chen Xi, Saishuai Dai, Chunyan Ji, and Margot Cocard. 2021. "Wave energy extraction for an array of dual-oscillating wave surge converter with different layouts." *Applied Energy* 292:116899.
- Contardo, Stephanie, Ron Hoeke, Mark Hemer, Graham Symonds, Kathy McInnes, and Julian O'Grady. 2018. "In situ observations and simulations of coastal wave field transformation by wave energy converters." *Coastal Engineering* 140:175–188. <https://doi.org/10.1016/j.coastaleng.2018.07.008>.

- De Andrés, AD, R Guanche, J Weber, and R Costello. 2015. "Finding gaps on power production assessment on WECs: Wave definition analysis." *Renewable Energy* 83:171–187. <https://doi.org/10.1016/j.renene.2015.04.026>.
- Ford, J.K.B. 1987. *A catalogue of underwater calls produced by killer whales (Orcinus orca) in British Columbia*. Technical report 633. Pacific Biological Station, Nanaimo, British Columbia V9R 5K6: Canadian Department of Fisheries and Oceans, Fisheries Research Branch, January.
- Francois, R. E., and G. R. Garrison. 1982a. "Sound absorption based on ocean measurements: Part I: Pure water and magnesium sulfate contributions." *Journal of the Acoustical Society of America* 72 (3): 896–907. <https://doi.org/10.1121/1.388170>.
- . 1982b. "Sound absorption based on ocean measurements. Part II: Boric acid contribution and equation for total absorption." *Journal of the Acoustical Society of America* 72 (6): 1879–1890. <https://doi.org/10.1121/1.388673>.
- Giassi, Marianna, Jens Engström, Jan Isberg, and Malin Götteman. 2020. "Comparison of wave energy park layouts by experimental and numerical methods." *Journal of Marine Science and Engineering* 8 (10): 750.
- Guerra, Maricarmen, and Jim Thomson. 2019. "Wake measurements from a hydrokinetic river turbine." *Renewable Energy* 139:483–495. <https://doi.org/https://doi.org/10.1016/j.renene.2019.02.052>.
- Hastie, G.D., D.J.F. Russell, P. Lepper, J. Elliott, B. Wilson, S. Benjamins, and D. Thompson. 2018. "Harbour seals avoid tidal turbine noise: Implications for collision risk." *Journal of Applied Ecology* 55 (2): 684–693. <https://doi.org/10.1111/1365-2664.12981>.
- Herbers, T.H.C., and T.T. Janssen. 2016. "Lagrangian Surface Wave Motion and Stokes Drift Fluctuations." *Journal of Physical Oceanography* 46:1009–1021. <https://doi.org/10.1175/JPO-D-15-00129.1>.
- Herbers, T.H.C., P.F. Jessen, T.T. Janssen, D.B. Colbert, and J.H. MacMahan. 2012. "Observing ocean surface waves with GPS-tracked buoys." *Journal of Atmospheric and Oceanic Technology* 29:944–959. <https://doi.org/10.1175/JTECH-D-11-00128.1>.
- Holt, M.M., D.P. Noren, V. Veirs, C.K. Emmons, and S. Veirs. 2009. "Speaking up: Killer whales (*Orcinus orca*) increase their call amplitude in response to vessel noise." *The Journal of the Acoustical Society of America* 125 (1): EL27–EL32. <https://doi.org/10.1121/1.3040028>.
- Howe, B.M., J. Miksis-Olds, E. Rehm, H. Sagen, P.F. Worcester, and G. Haralabus. 2019. "Observing the Oceans Acoustically." *Frontiers in Marine Science* 6:426. <https://doi.org/10.3389/fmars.2019.00426>.
- Joslin, J.B., E. Cotter, P.G. Murphy, P.J. Gibbs, R.J. Cavagnaro, C.R. Crisp, A.R. Stewart, et al. 2019. "The wave-powered adaptable monitoring package: hardware design, installation, and deployment." In *Proceedings of the 13th European Wave and Tidal Energy Conference*, 10. Napoli, Italy.

- Kerbiriou, Marie-Aurélie, Marc Prevosto, Christophe Maisondieu, Aurélien Babarit, and Alain Clément. 2007. "Influence of an improved sea-state description on a wave energy converter production." In *International Conference on Offshore Mechanics and Arctic Engineering*, 42711:463–473.
- Kohout, Alison L., Bill Penrose, Scott Penrose, and Michael J.M. Williams. 2015. "A device for measuring wave-induced motion of ice floes in the Antarctic marginal ice zone." *Annals of Glaciology* 56 (69): 415–424. <https://doi.org/10.3189/2015AoG69A600>.
- Kuik, A.J., G.P.H. Van Vledder, and L.H.Holthuijsen. 1988. "A Method for the Routine Analysis of Pitch-and-Roll Buoy Wave Data." *Journal of Atmospheric and Oceanic Technology* 18:1020–1034.
- Li, Y., and S.M. Çalişal. 2010. "Numerical analysis of the characteristics of vertical axis tidal current turbines." *Renewable Energy* 35 (2): 435–442. <https://doi.org/10.1016/j.renene.2009.05.024>.
- Lloyd, T.P., S.R. Turnock, and V.F. Humphrey. 2014. "Assessing the influence of inflow turbulence on noise and performance of a tidal turbine using large eddy simulations." *Renewable Energy* 71:742–754. ISSN: 0960-1481. <https://doi.org/10.1016/j.renene.2014.06.011>.
- Longuet-Higgins, M.S., D.E. Cartwright, and N.D. Smith. 1963. "Observations of the directional spectrum of sea waves using the motions of a floating buoy." *Ocean wave spectra*.
- Lossent, J., M. Lejart, T. Folegot, D. Clorennec, L. Di Iorio, and C. Gervaise. 2018. "Underwater operational noise level emitted by a tidal current turbine and its potential impact on marine fauna." *Marine Pollution Bulletin* 131:323–334. <https://doi.org/10.1016/j.marpolbul.2018.03.024>.
- Malinka, C.E., D.M. Gillespie, J.D.J. Macaulay, R. Joy, and C.E. Sparling. 2018. "First *in situ* passive acoustic monitoring for marine mammals during operation of a tidal turbine in Ramsey Sound, Wales." *Marine Ecology Progress Series* 590:246–266. <https://doi.org/10.3354/meps12467>.
- Melinger, D.K., K.M. Stafford, S.E. Moore, R.P. Dziak, and H. Matsumoto. 2007. "An Overview of Fixed Passive Acoustic Observation Methods for Cetaceans." *Oceanography* 20 (4): 36–45. <http://www.jstor.org/stable/24860138>.
- O'Reilly, W.C., T.H.C Herbers, R.J. Seymour, and R.T.Guza. 1996. "A Comparison of Directional Buoy and Fixed Platform Measurements of Pacific Swell." *Journal of Atmospheric and Oceanic Technology* 13:231–238.
- Pearman, D.W., T.H.C. Herbers, T.T. Janssen, H.D. Ettinger, S.A. McIntyre, and P.F. Jessen. 2014. "Drifter observations of the effects of shoals and tidal-currents on wave evolution in San Francisco Bight." *Continental Shelf Research* 91:109–119. <https://doi.org/10.1016/j.csr.2014.08.011>.
- Pedersen, Torstein, and Atle Lohrmann. 2004. "Possibilities and limitations of acoustic surface tracking." In *Oceans' 04 MTS/IEEE Techno-Ocean'04 (IEEE Cat. No. 04CH37600)*, 3:1428–1434. IEEE.
- Pedersen, Torstein, Eric Siegel, and Jon Wood. 2007. "Directional wave measurements from a subsurface buoy with an acoustic wave and current profiler (AWAC)." In *OCEANS 2007*, 1–10. IEEE.

- Polagye, B., and C Bassett. 2020. “Risk to marine animals from underwater noise generated by marine renewable energy devices.” In *OES-Environmental 2020 State of the Science Report: Environmental Effects of Marine Renewable Energy Development Around the World*, edited by A.E. Copping and L.G. Hemery, 67–85. Report for Ocean Energy Systems (OES). <https://doi.org/10.2172/1633082>.
- Polagye, B., and P. Murphy. 2015. “Acoustic Characterization of a Hydrokinetic Turbine.” In *Proceedings of the 11th European Wave and Tidal Energy Conference*, 7. Nantes, France.
- Rabault, Jean, Graig Sutherland, Olav Gundersen, Atle Jensen, Aleksey Marchenko, and Oyvind Breivik. 2020. “An open source, versatile, affordable waves in ice instrument for scientific measurements in the Polar Regions.” *Cold Regions Science and Technology* 170. <https://doi.org/10.1016/j.coldregions.2019.102955>.
- Riera, A., J.F. Pilkington, J.K.B Ford, E.H. Stredulinsky, and N.R. Chapman. 2019. “Passive acoustic monitoring off Vancouver Island reveals extensive use by at-risk Resident killer whale (*Orcinus orca*) populations.” *Endangered Species Research* 39:221–234. <https://doi.org/10.3354/esr00966>.
- Risch, D., N. van Geel, D. Gillespie, and B. Wilson. 2020. “Characterisation of underwater operational sound of a tidal stream turbine.” *The Journal of the Acoustical Society of America* 147 (4): 2547–2555. <https://doi.org/10.1121/10.0001124>.
- Saulnier, Jean-Baptiste, Alain Clément, F de O António, Teresa Pontes, Marc Prevosto, and Pierpaolo Ricci. 2011. “Wave groupiness and spectral bandwidth as relevant parameters for the performance assessment of wave energy converters.” *Ocean Engineering* 38 (1): 130–147. <https://doi.org/10.1016/j.oceaneng.2010.10.002>.
- Schmitt, P., B. Elsaesser, M. Coffin, J. Hood, and R. Starzmann. 2015. “Field Testing a Full-Scale Tidal Turbine Part 3: Acoustic Characteristics.” In *Proceedings of the 11th European Wave and Tidal Energy Conference*, 7. Nantes, France.
- So, Ratanak, Carlos Michelen, Bret Bosma, Pukha Lenee-Bluhm, and Ted KA Brekken. 2017. “Statistical analysis of a 1: 7 scale field test wave energy converter using WEC-sim.” *IEEE Transactions on Sustainable Energy* 8 (3): 1118–1126.
- Stratigaki, Vasiliki, Peter Troch, Tim Stallard, David Forehand, Jens Peter Kofoed, Matt Folley, Michel Benoit, Aurélien Babarit, and Jens Kirkegaard. 2014. “Wave basin experiments with large wave energy converter arrays to study interactions between the converters and effects on other users in the sea and the coastal area.” *Energies* 7 (2): 701–734. <https://doi.org/10.3390/en7020701>.
- Teng, Chung-Chu. 2002. “Wave Measurements from NDBC Buoys and C-MAN Stations,” <https://doi.org/0-7803-7534-3>.
- Thomsen, F., D. Franck, and J.K.B. Ford. 2001. “Characteristics of whistles from the acoustic repertoire of resident killer whales (*Orcinus orca*) off Vancouver Island, British Columbia.” *The Journal of the Acoustical Society of America* 109 (3): 1240–1246. <https://doi.org/10.1121/1.1349537>.

- Thomson, J. 2012. “Wave Breaking Dissipation Observed with “SWIFT” Drifters.” *Journal of Atmospheric and Oceanic Technology* 29:1866–1882. <https://doi.org/10.1175/JTECH-D-12-00018.1>.
- Thomson, J., E.A. D’Asaro, M.F. Cronin, W.E. Rogers, R.R. Harcourt, and A. Shcherbina. 2013. “Waves and the equilibrium range at Ocean Weather Station P.” *Journal of Geophysical Research: Oceans* 118:5951–5962. <https://doi.org/10.1002/2013JC008837>.
- Thomson, J., James B. Girton, Rajesh Jha, and Andrew Trapani. 2018. “Measurements of Directional Wave Spectra and Wind Stress from a Wave Glider Autonomous Surface Vehicle.” *Journal of Atmospheric and Oceanic Technology* 35:347–363. <https://doi.org/10.1175/JTECH-D-17-0091.1>.
- Thomson, J., and M. Guerra. 2018. *ORPC RivGen Hydrokinetic Turbine Wake Characterization*. Data retrieved from the Marine and Hydrokinetic Data Repository. doi: 10.15473/1432537.
- Thomson, J., J. Talbert, A. DeKlerk, A. Brown, and M. Schwendeman. 2015. “Biofouling Effects on the Response of a Wave Measurement Buoy in Deep Water.” *Journal of Atmospheric and Oceanic Technology* 32:1281–1286. <https://doi.org/10.1175/JTECH-D-15-0029.1>.
- Van Parijs, S.M., C.W. Clark, R.S. Sousa-Lima, S.E. Parks, S. Rankin, D. Risch, and I.C. Van Opzeeland. 2009. “Management and research applications of real-time and archival passive acoustic sensors over varying temporal and spatial scales.” *Marine Ecology Progress Series* 395:21–39. <https://doi.org/10.3354/meps08123>.
- Windt, Christian, Josh Davidson, and John V Ringwood. 2018. “High-fidelity numerical modelling of ocean wave energy systems: A review of computational fluid dynamics-based numerical wave tanks.” *Renewable and Sustainable Energy Reviews* 93:610–630.
- Wolgamot, Hugh A, and Colm J Fitzgerald. 2015. “Nonlinear hydrodynamic and real fluid effects on wave energy converters.” *Proceedings of the Institution of Mechanical Engineers, Part A: Journal of Power and Energy* 229 (7): 772–794. <https://doi.org/10.1177/0957650915570351>.
- Yu, Yi-Hsiang, and Ye Li. 2013. “Reynolds-Averaged Navier–Stokes simulation of the heave performance of a two-body floating-point absorber wave energy system.” *Computers & Fluids* 73:104–114. <https://doi.org/10.1016/j.compfluid.2012.10.007>.

Pacific Northwest National Laboratory

902 Battelle Boulevard
P.O. Box 999
Richland, WA 99352
1-888-375-PNNL (7675)

www.pnnl.gov